

# Synchronized Transform-Limited Operation of 10-GHz Colliding Pulse Mode-Locked Laser

C. Ji, N. Chubun, R. G. Broeke, J. Cao, Y. Du, S. J. B. Yoo, *Senior Member, IEEE*, K. Y. Liou, J. R. Lothian, S. Vatanapradit, S. N. G. Chu, B. Patel, W. S. Hobson, and W. T. Tsang

**Abstract**—We report a 10-GHz colliding pulse mode-locked laser fabricated with integrated active-passive waveguides. The laser fabrication adopted a deep reactive ion etching and single-step metal-organic vapor phase epitaxy regrowth process for forming the buried heterostructure waveguide. Clean output pulses resulted from laterally tilting the active-passive interface and effectively suppressing residual back-reflections at the interface. Hybrid mode-locking resulted in a synchronized transform-limited  $\text{sech}^2$  optical waveform. Pulswidth, chirp, timing jitter, and frequency-locking range were investigated through systematic device biasing condition optimization.

**Index Terms**—Active-passive integration, colliding pulse mode-locked (CPM) laser, frequency-locking range, hybrid mode-locking (HML), timing jitter, transform-limited pulse.

SEMICONDUCTOR mode-locked lasers are very attractive ultracompact sources for short optical pulse generation, with applications in high-speed optical data processing, optical time-division-multiplexed communication systems [1], and integrated photonic microsystems [2], with short unchirped pulses and low timing jitter as important requirements. For synchronized laser output with reduced timing jitter, electrical hybrid mode-locking (HML) at the fundamental or a subharmonic frequency [3], [4] provides a simpler optical setup over optical injection-locking approaches [5]. Lower repetition rate mode-locked lasers around 10 GHz are also desirable for relaxing the cost and complexity of electronics and important for lower bit rate applications. The optically pumped vertical-external-cavity surface-emitting laser [6] design realized 10-GHz transform-limited output, but required external cavity with dispersion compensation elements and off-chip SESAME absorber. Standard long cavity all-active mode-locked lasers for achieving the lower repetition rate tend to suffer from strong pulse shaping effects resulting in strongly chirped broad pulse and enhanced noise level [7]–[10]. With active-passive integration, these effects can be reduced; however, residual interfacial back-reflection can seriously degrade the mode-locking performance [3], [11].

Manuscript received July 15, 2005; revised November 26, 2005. This work was supported in part by Defense Advanced Research Projects Agency (DARPA) and by SPAWAR under agreement N66001-02-1.

C. Ji, N. Chubun, R. G. Broeke, J. Cao, Y. Du, and S. J. B. Yoo are with the Department of Electrical and Computer Engineering, University of California, Davis, CA 95616 USA (e-mail: yoo@ece.ucdavis.edu).

K. Y. Liou, J. R. Lothian, S. Vatanapradit, S. N. G. Chu, B. Patel, W. S. Hobson, and W. T. Tsang are with Multiplex, Inc., South Plainfield, NJ 07080 USA.

Digital Object Identifier 10.1109/LPT.2006.870185

Colliding pulse mode-locked (CPM) lasers first demonstrated in the external cavity configuration [12] and later monolithically [1], offer deeper saturation of the saturable absorber (SA) and more effective pulse narrowing compared to traditional mode-locked lasers. This letter discusses the fabrication and the performance of a 10-GHz CPM laser with an integrated active-passive waveguide demonstrating reduced pulse shaping and chirping effects. In contrast to previously reported low-repetition rate CPM laser designs [3], [7], our design utilizes only one pair of symmetric gain sections sandwiching the central SA section for simplified biasing control and reduced number of active-passive interfaces. The integrated waveguide employed a laterally tilted interface, which significantly reduces residual interfacial reflections, resulting in clean output pulses. We also adopted a simple and robust buried heterostructure (BH) waveguide formation process involving deep reactive ion etching (RIE) and a subsequent metal-organic vapor phase epitaxy (MOVPE) regrowth. We report for the first time, synchronized, transform-limited, and low jitter 10-GHz CPM operation under HML. Systematic investigations of dc and radio-frequency (RF) device biasing conditions for optimizing pulswidth, chirp, and timing jitter performance are also reported in detail.

The CPM laser fabrication process started on an MOVPE-grown InP wafer with an epitaxial-structure consisting of a 2- $\mu\text{m}$ -thick n-type InP lower cladding layer, an n-type 0.5- $\mu\text{m}$ -thick InGaAsP quaternary waveguiding layer of bandgap wavelength 1.15  $\mu\text{m}$  (1.15 $Q$ ), and a six (6-nm In<sub>0.53</sub>Ga<sub>0.47</sub>As) quantum-well active region. A 250-nm SiO<sub>2</sub> layer deposited by plasma-enhanced chemical vapor deposition (PECVD) underwent photolithography and RIE to define the 2000  $\times$  20  $\mu\text{m}^2$  active section. Outside this region not covered by SiO<sub>2</sub> pattern, selective wet etching removed the six quantum wells to expose the passive waveguide sections. After the SiO<sub>2</sub> mask removal, a thin (100 nm) undoped InP layer, a 2- $\mu\text{m}$ -thick p-type InP cladding layer, and a 100-nm-thick highly doped p-type InGaAs contact layer were MOVPE regrown across the entire wafer. The continuous waveguiding layer under the active region allowed the waveguide mode to propagate through the active-passive interface with minimal coupling loss and back-reflection.

The subsequent waveguide formation consisted of masking the ridge with a 250-nm patterned PECVD SiO<sub>2</sub> layer, while a methane-hydrogen-based RIE process deep etched the laser ridge past the 1.15 $Q$  waveguiding layer. An MOVPE regrowth process then covered the waveguide sidewalls with a regrown 2- $\mu\text{m}$ -thick Fe-doped InP layer. This relatively simple process created a BH structure with only a single regrowth step, and

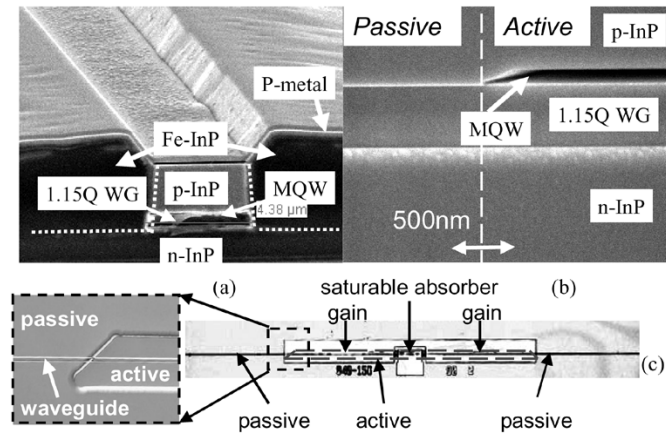


Fig. 1. (a) SEM cross-sectional view of the BH waveguide. (b) Cross-sectional view of the active-passive interface. (c) Top view of the central section of the CPM laser. Dashed line shows trapezoid-shaped active section (inset shows SEM of regrown active-passive interface before BH formation).

providing sidewall passivation, planarization, and electrical insulation. Subsequent processes included standard lapping, p- and n-type metallizations, and rapid-thermal-annealing. Fig. 1(a) shows the cross-sectional view of the BH ridge. Wet etching removal of the p-InGaAs layer in the 15- $\mu\text{m}$  gap between the gain and SA resulted in 11-k $\Omega$  electrical isolation for the 4- $\mu\text{m}$  waveguide, while the passive waveguide loss was 4 dB/cm.

Fig. 1(b) shows the cross-sectional view along the laser ridge revealing a very smooth interface between the active and the passive sections. Fig. 1(c) shows the top view of the fabricated CPM laser. The 2000- $\mu\text{m}$  trapezoidal shaped active region in the middle of the cavity consists of two gain sections sandwiching the 45- $\mu\text{m}$ -wide central SA section. Passive waveguides extend the active section in both directions to complete the symmetric 8200- $\mu\text{m}$ -long laser cavity. The active-passive interface was laterally tilted at 45 $^\circ$  to the waveguide orientation [110], allowing the TE waveguide mode to be incident at nearly Brewster's angle (with  $\Delta n_{\text{eff}} = 0.035$  between the active and passive sections) for reduced back-reflection. This eliminates unwanted secondary pulses and compound cavity spectral modes observed in our test lasers with untilted interfaces, which could cause undesirable system performance degradations [2].

For device characterizations, two dc needle probes forward biased the gain sections, while an RF ground-signal-ground probe applied the dc reverse bias voltage and the RF modulation signal to the SA section. A lensed fiber collected the CPM laser output, which after passing through an optical isolator, was amplified with a dispersion compensated erbium-doped fiber amplifier and routed to an optical spectrum analyzer, a 50-GHz digital sampling scope, a 40-GHz RF spectrum analyzer, and an autocorrelator for further analyses.

The laser operated passively mode-locked with the gain sections biased at 153 mA and the SA section biased at -8.4 V, emitting 3.0-ps-wide pulses with a time-bandwidth product of 0.43. Applying RF modulations to the SA resulted in output synchronization to the RF source, at both the fundamental CPM (10.3 GHz) frequency and the  $N = 2$  subharmonic hybrid mode-locking (SHML) frequency (5.15 GHz), with the  $N = 2$

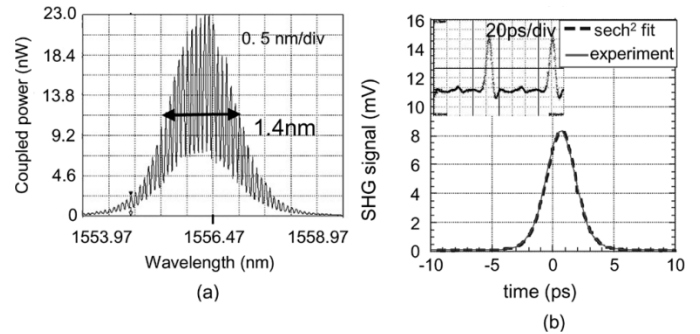


Fig. 2. (a) Optical spectrum and corresponding (b) autocorrelation trace fitted to a  $\text{sech}^2$  waveform under optimal biasing condition showing clean transform-limited output (19-dBm RF power at 10.300 GHz, SA biased at -9.2 V, gain section current at 150 mA). Inset in (b) shows sampling scope trace.

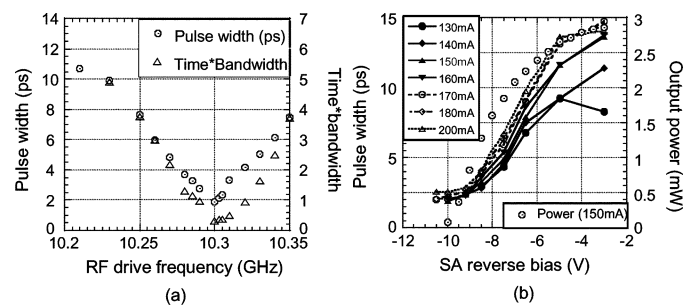


Fig. 3. Pulsewidth optimization showing (a) pulsewidth and time-bandwidth product as function of RF drive frequency at 19-dBm power; (b) pulsewidth as function of SA reverse biasing voltage and gain section current, and output power at 150 mA, at optimal RF biasing condition of (a).

SHML exhibiting low amplitude modulation distortion (>25 dB below the fundamental) [4]. The rest of the letter focuses on the detailed investigations of the fundamental HML case.

We systematically optimized the output pulse by iteratively adjusting in sequence the RF power, frequency, and the dc biasing conditions of the gain section current and the SA biasing voltage, respectively. Fig. 2(a) shows the optical spectrum with 1.4-nm spectral full-width at half-maximum (FWHM) at the final biasing condition after minimizing pulsewidth. Fig. 2(b) shows that the autocorrelation trace can be well fitted to a  $\text{sech}^2$  waveform, with an extracted FWHM of 1.84 ps, while Fig. 2(b) (inset) shows the stable sampling scope trace triggered with the RF source, showing good CPM output synchronization. The time-bandwidth product of 0.32 is very close to the theoretical transform-limited value for a  $\text{sech}^2$  waveform, without additional off-chip dispersion compensation [9]. This indicates that the CPM laser with active-passive integration overall suffered insignificant amount of chirping induced by self-phase modulation effect in the gain sections [8], [10].

Fig. 3(a) shows both the pulsewidth and the time-bandwidth product increasing rapidly with detuning of the RF drive frequency. Increased time-bandwidth product indicated that the detuning introduced significant chirp in the output pulse. Fig. 3(b) shows the pulsewidth dependence on the dc biasing conditions and output power at 150 mA at the optimal RF biasing condition in Fig. 3(a). The pulsewidth showed strong dependence on the SA reverse biasing voltage, dropping rapidly with increasing

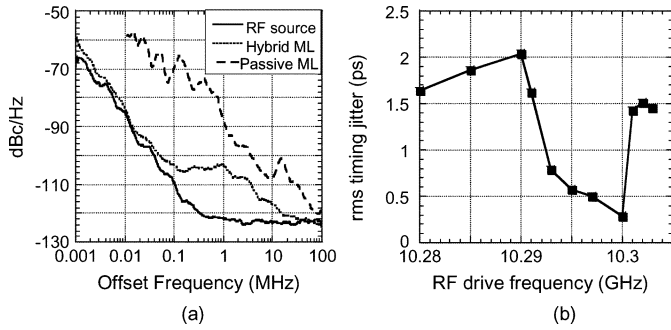


Fig. 4. (a) SSB phase noise spectra at CPM frequency. (b) RMS timing jitter as function of RF drive frequency under HML.

reverse biasing at low biasing levels while saturating at higher level. The pulsewidth also showed a gradual broadening with increasing gain current. The optimal biasing condition of Fig. 2 corresponded to low-gain-current and high SA-reverse-voltage biasing which occurred slightly above the threshold. The pulse shaping in a CPM laser involves the complex interplay of pulse broadening in the gain sections and pulse sharpening mechanisms in the SA sections [10]. Increasing SA reverse biasing voltage resulted in faster carrier sweep-out, more efficient pulse shaping, and shorter pulses. On the other hand, self-phase modulation effects in the gain section increased moderately with higher gain biasing and introducing additional pulse broadening. Further reduction of the pulsewidth can be expected with cavity  $Q$  increase through high reflection coating [5], compensating for the passive waveguide loss.

Fig. 4(a) shows the single sideband (SSB) phase noise plot centered at 10.3 GHz, comparing the optimal HML condition of Fig. 2, the passive mode-locking, the RF source (HP8350B) noise floor. The root-mean-square (rms) timing jitter estimation included phase noise integration from 20 k to 80 MHz, corresponding to the ITU measurement filter at 10 GHz [9]. For an RF source background of 0.199 ps, the CPM laser under optimal HML had rms jitter of 0.283 ps, while the corresponding passive mode-locking case showed timing jitter of 3.6 ps. Fig. 4(b) shows the timing jitter of the HML case as a function of the RF drive frequency. A frequency-locking range of  $\sim 7$  MHz with lower jitter was observed, with the minimal jitter condition at 10.3 GHz also matching the optimized biasing condition of Fig. 2. This indicated that with a systematic biasing condition optimization, optimal 10-GHz CPM laser output pulses with minimal pulsewidth, chirp, and timing jitter are simultaneously achieved.

The asymmetric-locking range in Fig. 4(b) is likely related to amplitude and timing instability associated with cyclic wavelength variations, as observed in active mode-locked lasers [13]. Another possible effect is due to the linewidth enhancement  $\alpha$ -factor. Mode-locking at the detuned RF drive frequency implies the cavity resonance frequency should shift accordingly, which causes the gain section carrier density and

index to change through the carrier plasma effect. Negative frequency detuning requires increased refractive index, which reduces the carrier density and gain due to the  $\alpha$ -factor. Positive frequency detuning requires increased carrier population and gain. The laser's preference for the lowest gain state would make the negative detuning locking the more stable condition compared to the unlocked state, contributing to the asymmetric locking curve.

In summary, we report BH CPM lasers fabricated with a simple MOVPE single-step regrowth-based process, and active-passive integrated waveguide for reducing the pulse shaping effects. Clean output pulses resulted from a  $45^\circ$  laterally tilted active-passive interface. We demonstrated synchronized transform-limited  $\text{sech}^2$  output pulse with relatively low timing jitter at 10.3 GHz, and investigated biasing condition dependence of pulsewidth, chirp, and the frequency-locking range.

#### REFERENCES

- [1] Y. K. Chen, M. C. Wu, T. Tanbun-Ek, R. A. Logan, and M. A. Chin, "Subpicosecond monolithic colliding-pulse mode-locked multiple quantum well lasers," *Appl. Phys. Lett.*, vol. 58, pp. 1253–1255, 1991.
- [2] C. Ji, R. G. Broeke, Y. Du, C. Jing, N. Chubun, P. Bjeletich, F. Olsson, S. Lourudoss, R. Welty, C. Reinhardt, P. L. Stephan, and S. J. B. Yoo, "Monolithically integrated InP-based photonic chip development for O-CDMA systems," *IEEE J. Sel. Topics Quantum Electron.*, vol. 11, no. 1, pp. 66–77, Jan./Feb. 2005.
- [3] H. Fan, C. Wu, M. El-Aasser, N. K. Dutta, U. Koren, and A. B. Piccirilli, "Colliding pulse mode-locked laser," *IEEE Photon. Technol. Lett.*, vol. 12, no. 8, pp. 972–973, Aug. 2000.
- [4] T. Hoshida, H. F. Liu, M. Tsuchiya, Y. Ogawa, and T. Kamiya, "Subharmonic hybrid mode-locking of a monolithic semiconductor laser," *IEEE J. Sel. Topics Quantum Electron.*, vol. 2, no. 3, pp. 514–522, Sep. 1996.
- [5] S. Arahira and Y. Ogawa, "480-GHz subharmonic synchronous mode locking in a short-cavity colliding-pulse mode-locked laser diode," *IEEE Photon. Technol. Lett.*, vol. 14, no. 4, pp. 537–539, Apr. 2002.
- [6] A. Aschwanden, D. Lorenser, H. J. Unold, R. Paschotta, E. Gini, and U. Keller, "10 GHz passively mode-locked external-cavity semiconductor laser with 1.4 W average output power," *Appl. Phys. Lett.*, vol. 86, pp. 131 102–1–3, 2005.
- [7] C. J. K. Richardson and J. Goldhar, "Solid-state repetition-rate tunable semiconductor colliding-pulse mode-locked laser," *IEEE Photon. Technol. Lett.*, vol. 16, no. 4, pp. 978–980, Apr. 2004.
- [8] D. J. Derickson, P. A. Morton, J. E. Bowers, and R. L. Thornton, "Comparison of timing jitter in external and monolithic cavity mode-locked semiconductor lasers," *Appl. Phys. Lett.*, vol. 59, pp. 3372–3374, 1991.
- [9] K. Yvind, D. Larsson, L. J. Christiansen, J. Mork, J. M. Hvam, and J. Hanberg, "High-performance 10 GHz all-active monolithic modelocked semiconductor lasers," *Electron. Lett.*, vol. 40, pp. 735–737, 2004.
- [10] S. Bischoff, M. P. Sorensen, J. Mork, S. D. Brorson, T. Franck, J. M. Nielsen, and A. Moller-Larsen, "Pulse-shaping mechanism in colliding-pulse mode-locked laser diodes," *Appl. Phys. Lett.*, vol. 67, pp. 3877–3879, 1995.
- [11] P. B. Hansen, G. Raybon, U. Koren, P. P. Iannone, B. I. Miller, G. M. Young, M. A. Newkirk, and C. A. Burrus, "InGaAsP monolithic extended-cavity lasers with integrated saturable absorbers for active, passive, and hybrid mode locking at 8.6 GHz," *Appl. Phys. Lett.*, vol. 62, pp. 1445–1447, 1993.
- [12] J. P. van der Ziel, R. A. Logan, and R. M. Mikulyak, "Generation of subpicosecond pulses from an actively mode locked GaAs laser in an external ring cavity," *Appl. Phys. Lett.*, vol. 39, pp. 867–869, 1981.
- [13] A. J. Lowery, N. Onodera, and R. S. Tucker, "Stability and spectral behavior of grating controlled actively mode locked lasers," *IEEE J. Quantum Electron.*, vol. 27, no. 11, pp. 2422–2430, Nov. 1991.